



# Characterization of nanocellulose- reinforced shape memory polyurethanes

Mar'ia L Auad,<sup>1</sup> Vasili S Contos,<sup>2</sup> Steve Nutt,<sup>2</sup> Mirta I Aranguren<sup>3</sup> and Norma E Marcovich<sup>3\*</sup>

<sup>1</sup>Polymer and Fiber Engineering, Auburn University, 103 Textile Building, Alabama, USA

<sup>2</sup>Chemical Engineering and Materials Science Department, University of Southern California, Gill Foundation Composites Center, 3651 Watt Way, VHE-602, Los Angeles, California, USA

<sup>3</sup>INTEMA, Chemical Engineering Department, UNMDP-CONICET, Juan B Justo 4302, Mar del Plata, Argentina

\* E-mail address: marcovic@fi.mdp.edu.ar

## Abstract:

**BACKGROUND:** Shape memory polymers are capable of fixing a transient shape and of recovering their original dimensions by the application of an external stimulus. Their major drawback is their low stiffness compared to smart materials based on metals and ceramics. To overcome this disadvantage, nanocellulose was utilized as reinforcement.

**RESULTS:** Composites were prepared by casting stable nanocellulose/segmented polyurethane suspensions. The heat of melting of the polyurethane soft segment phase increased on cellulose addition. Composites showed higher tensile modulus and strength than unfilled films (53% modulus increase at 1 wt% nanocellulose), with higher elongation at break. Creep deformation decreased as cellulose concentration increased (36% decrease in 60-minute creep by addition of 1 wt% nanocellulose). The nanocomposites displayed shape memory properties equivalent to those of the neat polyurethane, with recoveries of the order of 95% (referred to second and further cycles).

**CONCLUSIONS:** It is possible to markedly improve the rigidity of shape memory polymers by adding small amounts of well-dispersed nanocellulose. However, this improvement did not have substantial effects on the material shape fixity or recovery. Shape memory behavior seems to

Please cite this article as: M. L. Auad, V. S. Contos, S. Nutt, M.I. Aranguen, and N.E. Marcovich, "Characterization of Nano-Cellulose Reinforced Shape Memory Polyurethanes," *Polymer International* 57 [4] (2008) 651-659. DOI: <http://dx.doi.org/doi:10.1002/pi.2394>



continue to be controlled by the polymer properties. Copyright © 2007 Society of Chemical Industry  
Key words: A-Short-Fibre Composites, C-Finite Element Analysis (FEA), C-Modelling, Mean-field homogenization

## 1. INTRODUCTION

Shape memory materials are the key components of intelligent/smart composites because of their unusual properties, such as shape memory behavior, pseudo-elasticity or large recoverable strain, high damping capacity and adaptive properties, which derive from reversible phase transitions in the materials.<sup>1</sup>

Shape memory polymers (SMPs) possess the ability to store and recover large strains by the application of a prearranged thermomechanical cycle. Thus, they can be fixed in a transient shape to subsequently recover their original one.<sup>2</sup> Because SMPs have large recoverable strain, are light, are easy to manipulate and are economical compared with shape memory alloys (SMAs), their development is being vigorously pursued.<sup>2-4</sup> In general, linear SMPs contain two phases: a thermally reversible phase responsible for fixing a transient shape and a frozen phase responsible for recovering the original shape. The fixed structures responsible for ‘remembering’ the original shape can consist of a crystalline phase, a glassy phase, an entanglement network or a crosslinking network. The thermally reversible phase is generally designed to have a large decrease in elastic modulus on heating through its phase transition temperature ( $T_s$ ).<sup>5</sup> Depending on the particular system, the phase transition of the reversible phase could be a melting temperature (if a crystalline phase is considered) or a glass transition (if dealing with an amorphous phase), and this particular transition can be used as  $T_s$ . Thus, when SMPs are heated to a temperature above that of the thermally reversible phase ( $T_s$ ), but below the phase transition temperature of the frozen phase, a large deformation can be

easily imposed due to the small modulus of the polymer. The deformation can also be fixed in a  
Please cite this article as: M. L. Auad, V. S. Contos, S. Nutt, M.I. Aranguen, and N.E. Marcovich, “**Characterization of Nano-Cellulose Reinforced Shape Memory Polyurethanes,**” *Polymer International* 57 [4] (2008) 651-659. DOI: <http://dx.doi.org/doi:10.1002/pi.2394>



subsequent cooling process because of the increase in modulus of the thermally reversible phase. Subsequently, the original shape can be recovered by heating above  $T_s$ , the phase transition temperature of the reversible phase, due to the elastic energy stored by the frozen phase.

Some of the most common polymers that exhibit shape memory behavior are segmented polyurethanes. These polyurethanes (PUs) are basically block copolymers of soft segments and hard segments. The soft segments are polyols, typically with number molecular weights of 1000–2000  $\text{g mol}^{-1}$ , whereas the hard segments are built from diisocyanates and extenders. Depending on the type and composition of the soft and hard segments and the preparation procedures, the structure–property relations of PUs can be extremely diverse, which offers the possibility of controlling them. Hence, the shape recovery temperature can be set at any temperature between  $-30$  and  $70$   $^{\circ}\text{C}$ , enabling a broad range of applications<sup>6</sup>

A major drawback of SMPs is their low stiffness compared to metals and ceramics.<sup>4</sup> The low stiffness of SMPs results in a relatively small recovery force under constraint (actuation force) compared to alternative active actuation materials or schemes.<sup>7</sup> Thus, in some applications, SMPs may not generate sufficient recovery force to be viable. To overcome this drawback, scientists have attempted to increase the recovery force of SMPs by adding reinforcements such as carbon or glass fibers, or ceramic filler particles to the polymer matrix.<sup>4,7</sup>

Another interesting behavior of polymers and polymer composites involves creep, the time-dependent deformation of materials subjected to a continuous stress.<sup>8</sup> Creep deformation has both elastic and plastic components, and therefore it can be non-recoverable when the load is removed. Creep can lead to unacceptable deformation and eventually to structural failure. It is, therefore, an important property for engineering plastics and composites.<sup>8</sup> Relatively poor creep resistance and low dimensional stability of thermoplastics are common deficiencies, impairing service life and



safety, and limiting applications. One of the ways to overcome this problem is, once more, the use of reinforcements, as demonstrated by Zhang et al.<sup>9</sup> These researchers showed that even a very low volume loading of nanoparticles substantially improved the creep resistance of a polyamide-6,6.

Taking into account the low concentrations of particles incorporated when fabricating polymer-based nanocomposites, particle dispersion and wetting are critical. These interrelated factors are influenced by the processing conditions and the chemistry of the base material, and can strongly affect the composite mechanical properties.<sup>4</sup> One of the most important factors affecting the reinforcing effect of the filler is adhesion of the polymer to the filler surface. Interfacial adhesion depends on the nature of the bonds at the polymer–solid phase boundary. The polymer–filler interaction leads to the development of localized stresses at the surface of filler particles and determines the characteristics of the deformation and breakdown of the filled polymer.<sup>10</sup>

Cellulose can be a source for polymer nanoreinforcements and it is one of the most abundant substances in nature, where it constitutes the primary structural material in a wide variety of plant life, as well as being present in some animal life.<sup>11</sup> In addition, the attributes of low cost, low density, high stiffness, consumable nature and biodegradability<sup>12–15</sup> constitute major incentives for exploring new uses. Moreover, cellulose has polar groups that can interact with polar polymers, such as PUs, leading to a composite material with good interfacial adhesion.<sup>16</sup> This is essential to enhance composite mechanical properties.

The aim of the work reported here was to study the effect of reinforcing shape memory PUs with nanocellulose crystals. The incorporation of nanoreinforcements into SMPs is expected to yield some performance benefits (such as an increase in the elastic modulus or a reduction in creep) at small nanoparticle loadings (ca 1 wt%), producing stiffer yet deformable composites with a deformation capability comparable to that of unfilled polymers.



## 2. MATERIALS AND METHODS

### 2.1. Materials

A high-performance polyester thermoplastic PU (IROGRAN PS455-203, Huntsman) was selected as the matrix. This linear segmented PU exhibits a low glass transition temperature ( $T_g = -36.5$  °C, determined by dynamic mechanical analysis, as the temperature of the maximum in  $\tan \delta$ ), near-ambient melting of soft-segment crystallites ( $T_{m,s} = 41$  °C, determined by DSC), high deformation (ca 650%, measured at a crosshead speed of  $100 \text{ mm min}^{-1}$ ) and strain-induced crystallization.

Cellulose nanocrystals were produced from commercial microcrystalline cellulose (MCC, Avicel PH-101, FMC BioPolymer, USA) by acid hydrolysis, using a method described elsewhere.<sup>16</sup> Henceforth, these will be referred to as nanocellulose to avoid confusion with the PU crystals. The reinforcement was dispersed in dimethylformamide (DMF) by ultrasonication (40 kHz, 160 W, TESTLAB ultrasonic bath, model TB04, Buenos Aires, Argentina) and subsequently incorporated into a DMF–PU solution. Films of reinforced PUs (about 0.5 mm in thickness) containing 0, 0.1, 0.5 and 1 wt% fibers were obtained by casting the mixture in an open mold and drying in a convection oven at 80 °C for 24 h.

### 2.2. Methods

SEM (Cambridge 360) was used to observe the fracture surfaces of the composite films pre-chilled in liquid nitrogen. Samples were sputter-coated with gold prior to SEM observation.

DSC testing of the samples was performed using a calorimeter (Perkin Elmer Pyris 1) equipped with a cooling unit, and operating under nitrogen atmosphere ( $20 \text{ mL min}^{-1}$ ). Measurements were performed at  $5 \text{ °C min}^{-1}$ . The average values of at least three replicates of each sample are reported.



The thermomechanical response of specific samples was determined using a rheometer (Anton Paar, Physica MCR 301). Tests were conducted using the temperature scan mode, applying a deformation of 0.05%. The frequency of the forced oscillations was fixed at 1 Hz. The specimens were cut to  $40 \times 5 \times 0.5 \text{ mm}^3$ , and the dimensions were measured with an accuracy of 0.01 mm. The maximum in  $\tan \delta$  was utilized to determine the temperature of the main relaxation associated with  $T_g$  of the polymer (soft segments).

To investigate the underlying microstructure of PUs and composites with different cellulose contents, wide-angle X-ray scattering (WAXS) was employed. The diffractograms were recorded using a Philips model PW 1830 X-ray diffractometer, with Ni-filtered  $\text{Co K}\alpha$  radiation at 40 kV and 30 mA. Samples were scanned from  $2\theta = 5$  to  $60^\circ$  in steps of  $0.02^\circ$ .

Tensile testing was performed at  $20^\circ\text{C}$  on microtensile specimens of  $5 \text{ mm} \times 25 \text{ mm}$  cut from the molded films, using a universal testing machine (Instron 8501), in accordance with ASTM D 1708. A crosshead speed of  $10 \text{ mm min}^{-1}$  was used. The average values of at least five replicates of each sample were reported. Experimentally determined Young's moduli were compared with theoretical predictions, as detailed below. Thus, the reinforcement volume content was calculated using  $1.53 \text{ g cm}^{-3}$  as the density of the cellulose crystals<sup>17</sup> and  $1.0 \text{ g cm}^{-3}$  as the density of the PU (experimental value).

In multiphase polymer systems, the relationship between the elastic moduli, the concentration of the two components and the morphologies (or geometrical arrangements of each phase) has been extensively studied.<sup>18</sup> One of the simplest models involves connections in series (Reuss prediction) or in parallel (Voigt prediction) of the components, and leads to the lowest lower bound (Eqn (1)) or the highest upper bound (Eqn (2)) for the moduli, respectively:<sup>18</sup>



$$E_c = \frac{1}{v_f/E_f + (1 - v_f)/E_m} \quad (1)$$

$$E_c = v_f E_f + (1 - v_f) E_m \quad (2)$$

where E is any modulus (shear, Young's or bulk) of the material, v is the volume fraction and the subscripts f and m refer to the filler and the matrix, respectively.

The theoretical model of Halpin–Kardos, also known as the mean field model, given by

$$E_c = \frac{1 + 2(L/D)\eta v_f}{1 - \eta v_f} E_m; \eta = \frac{E_f/E_m - 1}{E_f/E_m + 2(L/D)} \quad (3)$$

has been used extensively to predict the elastic modulus of short-fiber composites.<sup>19</sup> In this approach, fibers are assumed to be smeared in the matrix, to form a homogeneous continuum, and thus no interaction between fibers is taken into account. The properties of the composite depend then on the size, shape and volume fraction of the fibers and on the mechanical properties of both matrix and fibers. Additionally, the model proposed by Pan<sup>20</sup> for fiber-reinforced composites with short fibers randomly oriented in three (three-dimensional) directions can be considered:

$$E_c = (v_f/2\pi)E_f + (1 - v_f/2\pi)E_m \quad (4)$$

Thermal cyclic tests were performed on microtensile specimens of 5 mm × 25 mm using a universal testing machine equipped with a heating chamber (Instron 8501). Samples were first conditioned at 60 °C for 10 min and subsequently elongated to 100% of the original length at a speed of 20 mm min<sup>-1</sup>. Then the samples were cooled to 30 °C and unloaded. Finally, the samples underwent the recovery process by heating for 10 min at 60 °C. The strain maintained after unloading and the residual strain of each cycle were used to calculate the fixity ( $R_f$ ) and recovery ( $R_r$ ) ratios from these tests, as indicated in the following equations:

$$R_f = \frac{\varepsilon_u}{\varepsilon_m} \times 100\% \quad (5)$$

$$R_r(N) = \frac{\varepsilon_m - \varepsilon_p(N)}{\varepsilon_m - \varepsilon_p(N-1)} \times 100\% \quad (6)$$



where  $\varepsilon_m$  is the maximum strain in the cycle (100%),  $\varepsilon_u$  is the residual strain after unloading at 30 °C and  $\varepsilon_p(N)$  represents the residual strain after heating at 60 °C in the N th cycle.

A dynamic mechanical analyzer (Perkin Elmer DMA 7) was used to perform short-time creep experiments (test duration of 60 min). The tests were carried out in creep mode using a tensile fixture. The sample dimensions were approximately  $20 \times 4.5 \times 0.5 \text{ mm}^3$  and the linear dimensions were measured up to 0.01 mm. A fixed stress of 500 kPa was applied for 60 min and then removed. The sample deformation was continuously recorded for 120 min. The temperature was maintained at 20 °C during the entire test.

### 3. RESULTS AND DISCUSSION

#### 3.1. SEM and analysis of nanocellulose dispersion

SEM micrographs obtained from cryo-fractured films are shown in Fig. 1. The fracture surface of the neat matrix is completely featureless (Fig. 1(a)), as expected for a monolithic homogeneous material. The small holes observed may be the result of retained bubbles during casting and drying of the films. A larger magnification (Fig. 1(b)) shows that the surface is smooth and clean. In contrast, Fig. 1(c) shows the fracture surface of a sample containing 1 wt% of nanocellulose, and in this case its appearance is qualitatively different. The surface is rougher, indicating increased energy dissipation during fracture, due to changes in crack trajectory. The explanation for this change in behavior is that the advancing crack must change its path (deflection) because of the presence of the rigid filler material, i.e. nanocellulose.

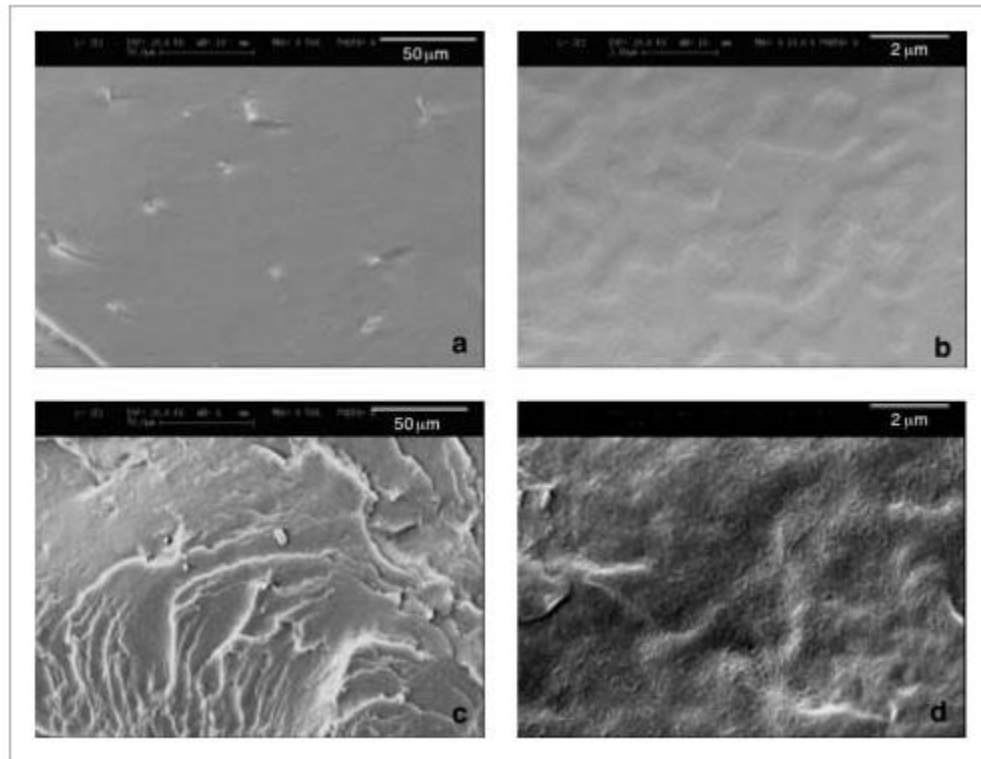


Figure 1. SEM micrographs of cryo-fractured samples: (a, b) unreinforced PU; (c, d) 1 wt% nanocellulose-reinforced PU.

A larger magnification of the cryo-fractured surface (Fig. 1(d)) allows the observation of a large number of fibrils spanning the whole area of the examined surface. This feature was observed only in filled films. At this concentration (1 wt%), the nanofibrils appear as interacting with (i.e. touching) one another. Although overlapping may occur, they seem to be well dispersed throughout the film. The thickness of the thinner fibrils is in the range 10–20 nm, although thicker fiber-like features are also present. Regarding the length of the fibrils, it is not possible to be sure that they are observed in their whole length since they may be laying at an angle to the fracture surface observed or may be crossed by other fibrils. In any case, the observed fibrils (or fiber-like aggregates) appear in the image as having lengths of the order of 150–1000 nm.



The presence of these surface features is an indication of the presence of nanocellulose throughout the sample.<sup>16</sup> Additionally, the size of the fiber-like features observed in Fig. 1(d) is comparable to the size of cellulose crystals, which has already been reported in a previous publication, and also by other authors, to be of 5–20 nm in diameter and of the order of hundreds of nanometers in length.<sup>16, 21, 22</sup> The thinner fibrils observed in the present work have the same size as that of cellulose nanocrystals characterized previously by AFM.<sup>16</sup> The thicker features are interpreted as the result of aggregation of the crystals, or as polymer-coated nanocellulose, or just the thickening expected from the metal sputtering used in SEM. The length of the features observed is well in the range expected for nanocellulose crystals, although, as indicated above, fibrils are difficult to individualize after being incorporated into the composite.

### 3.2. Characterization of PU and composite films

#### DSC measurements

Thermograms corresponding to the first heating of PU films with and without nanocellulose addition can be seen in Fig. S1 of the supplementary material. The melting of the soft segments is clearly seen, while the hard segment transition appears as a small deflection in the thermogram. The incorporation of small amounts of nanocellulose produces a measurable shift of the temperature of the melting of the soft segments towards higher temperatures (Table 1).



Table 1. Glass transition temperature ( $T_g$ ), melting temperature ( $T_m$ ) and heat of melting ( $\Delta H$ ) of cellulose-reinforced PU

Cellulose (wt%)	$T_g$ (°C)	$T_{m, s}$ (°C)	$T_{m, h}$ (°C)	$\Delta H_{m, s}$ (J g <sup>-1</sup> )	$\Delta H_{soft}/\Delta H_{softunfilled}$
0.0	-36.5	41.0 ± 1.5	136.6 ± 0.1	7.0 ± 0.5	1.0
0.1	-36.3	41.3 ± 0.7	139.7 ± 4.5	8.0 ± 0.3	1.2
0.5	-36.0	42.2 ± 0.2	142.4 ± 0.6	9.0 ± 0.4	1.3
1.0	-35.7	43.1 ± 0.4	139.4 ± 1.0	12.3 ± 0.2	1.8

Subscripts: s, soft segments; h, hard segments.

Additionally, Table 1 shows that the heat of melting of the soft segments ( $\Delta H_{m, s}$ ) is also affected by the presence of nanocellulose.  $\Delta H_{m, s}$  increases as the cellulose content increases, the heat measured for the 1 wt% sample being about 80% higher than that for unfilled PU.

The above results are indications that the cellulose favors crystallization and the betterment of the crystals since they melt at slightly higher temperatures in the nanocomposites. These observations can be ascribed to a possible anchoring effect of the filler, nanocellulose acting as a nucleating agent for the polymer crystallization. This behavior has also been noticed in other systems. Nunes et al.<sup>23</sup> observed that PU–silica interactions involved, preferentially, the polymer soft segments, resulting in less direct interactions between soft and hard phases. This, in turn, increases phase segregation and facilitates orientation and crystallization under tension. In other words, this behavior can be attributed to soft-segment alignment, resulting in direct interactions between silicates and PU segments and, similarly in the present case, with nanocellulose.

The above explanation can also be extended to the effect observed on the heat of melting of the soft segments, which indicates that the crystallization of the soft phase is favored with increasing cellulose concentration, and that chain mobility is not hindered to form increasingly better soft segment crystals (higher heat of melting and higher melting temperature). This behavior may stem from well-dispersed nanocellulose that maximizes matrix–cellulose interactions. As the cellulose content increases, the amount of fiber–matrix interfaces increases, favoring the soft polymer



segments phase segregation. In the case of the sample containing 1 wt% cellulose, the SEM image in Fig. 1(d) reveals a nanofibril network that completely spans the sample. In this case the interactions between nanocellulose and polymer are maximized, and thus the heat of fusion of the soft segments is the highest.

It is interesting to point out that a previous rheological study performed on a different and unreacted PU liquid mixture filled with different concentrations of nanocellulose indicated that the percolation threshold of the nanofibrils was around 1 wt%.<sup>16</sup> Thus, it would be expected that at the concentrations used here, there is little agglomeration present, and that large interfacial interaction matrix reinforcement could be developed.

#### Dynamic mechanical response of the films

The dependence of the loss tangent,  $\tan \delta$ , on temperature for different cellulose concentrations is shown in Fig. S2. Note that the main relaxation of the amorphous soft segment domains (related to the glass transition temperature of PU soft segments), as measured by the height and position of the  $\tan \delta$  peak, is sensitive to the presence of nanocellulose.  $T_g$  is to some extent higher in the reinforced material compared to the unreinforced polymer, and it seems to increase slightly as cellulose concentration increases (Table 1), although the observed differences are minor (and probably are within experimental error). The magnitude of the  $\tan \delta$  peak also allows one to make some interesting observations. Adding 0.1 wt% nanocellulose produces essentially no change in the height of the peak. However, the addition of 0.5–1 wt% cellulose substantially reduces the height of the peak, indicating that less material is taking part in the transition. However, the change is much larger than would be expected from a dilution effect with only 1 wt% of cellulose. This is another indication of the strong interfacial interactions developed between the nanocellulose and the polymer.



Other authors have also observed variations in  $T_g$  of polymeric matrices as nanofillers are incorporated. Gall et al.,<sup>4</sup> who worked on nanocomposites based on SiC nanoparticles and SMP PUs, indicated that these changes resulted from the alterations of the kinetics of the glass transition due to the presence of particles. Mathew and Dufresne<sup>24</sup> also noticed an increase in  $T_g$  with reinforcement content for starch–cellulose (tunicin) whisker nanocomposites. As in our case, they also observed a concomitant increase in the crystallinity of the starch with tunicin content. They ascribed the increase of  $T_g$  to the restricted mobility of amorphous polymer chains that results from the physical crosslinks induced by crystallization. The increase in  $T_g$  up to 15 wt% whisker addition was therefore explained as the direct outcome of the decrease in the flexibility of the polymer chains in the presence of both stiff crystalline whiskers and starch crystalline domains.

#### Crystallinity of neat PU and composite films

The pattern of the WAXS curves (Fig. S3) suggests that the materials contain different crystalline and amorphous phase states. The presence of a number of diffraction maxima (the most intense appearing at  $2\theta = 26.3^\circ$ ) in the scattering curve for the individual cellulose crystals demonstrates the existence of long-range order in the arrangement of atomic layers in the reinforcement. The pattern for the 1 wt% cellulose composite shows a weak peak at  $2\theta = 26.3^\circ$ , which reveals the presence of cellulose.

The pattern produced by neat PU exhibits a nearly symmetrical diffuse maximum at  $2\theta = 23.1^\circ$ , indicative of short-range (translational) ordering in the arrangement of chain fragments.<sup>25</sup> Neat polymer also exhibits a weak peak at  $2\theta = 24.1^\circ$ , which arises from a crystalline phase. The position of the peak shifts to slightly higher angles as the cellulose content increases (i.e.  $2\theta = 25.4^\circ$  for 1 wt% cellulose). This diffraction peak is related to the soft segment crystalline phase, since the position of



the diffraction peak for the hard segments (more easily observed in PU with high concentrations of hard segments) is in the range  $2\theta = 11\text{--}12^\circ$ .<sup>23</sup>

The observed shift in the diffraction peak of the soft segment crystalline phase is related to the interatomic separation (d-spacing) of the planes in the crystals. According to the results presented above, the maximum of the peak shifts to higher angles, indicating reduced interplanar spacing. Actually, if the soft segment crystalline phase is not well separated from the rest of the polymer, the resulting crystals are defective and the interplanar spacing in the crystals is disturbed and larger than that in better formed crystals. As a result, the peak in the WAXS pattern will appear at lower angles. If the phase separation is improved, the crystals will be more perfect, achieving an undisturbed lower interatomic spacing. Consequently, the crystalline peak shifts towards larger angles, as was observed after cellulose addition. These results and corresponding analysis are in excellent agreement with the information offered by DSC thermograms of the films. In that case, DSC scans also showed that the addition of nanocellulose leads to more perfect soft segment crystals (higher melting temperature).

#### Static tensile testing

Tensile stress–strain curves for the neat PU and nanocellulose composites are shown in Fig. S4. All the samples presented high elongation at break (more than 400%) and strain hardening, which is the result of strain-induced crystallization. The stress at yield of the material increases as the fiber content increases.

An elastomer must dissipate energy at an advancing crack tip in order to exhibit high tensile strength. Usually this is a viscoelastic process.<sup>10</sup> The strengthening effect of the filler derives from the dissipation of energy via viscoelastic processes, preventing the fractures reaching sizes at which they become unstable and propagate. In other words, in a reinforced polymer, when a growing crack



encounters a filler particle, energy dissipation occurs, and a higher increase in tension for further fracture growth is necessary. As a consequence, as filler concentration increases, the number of 'barriers' preventing crack growth increases and the rupture process is delayed. Additionally, it is known that agglomeration in poorly dispersed composites causes crack initiation and propagation, reducing the composite strength.<sup>26</sup> Since increasing tensile strength is observed with the addition of increasing concentrations of cellulose crystals, this can be considered an indirect indication of the relatively uniform dispersion of nanocellulose in the polymeric matrix. Again this observation is in good agreement with the nanofibril distribution observed in Fig. 1(d).

The tensile Young's moduli ( $E$ ) of the materials are presented in Fig. 2. As expected, the modulus increased with increasing filler content. Noticeably, the addition of only 1 wt% cellulose nanocrystals (which corresponds to 0.66 vol.%) produced a 53% increase in Young's modulus over that of the neat system. The observed increase in Young's modulus for the 1 wt% sample is rather large when compared to variations reported by other authors; for example Gall et al.<sup>4</sup> observed an increase of 300% in the modulus of a shape memory epoxy resin filled by SiC, but at concentrations as high as 40 wt%.

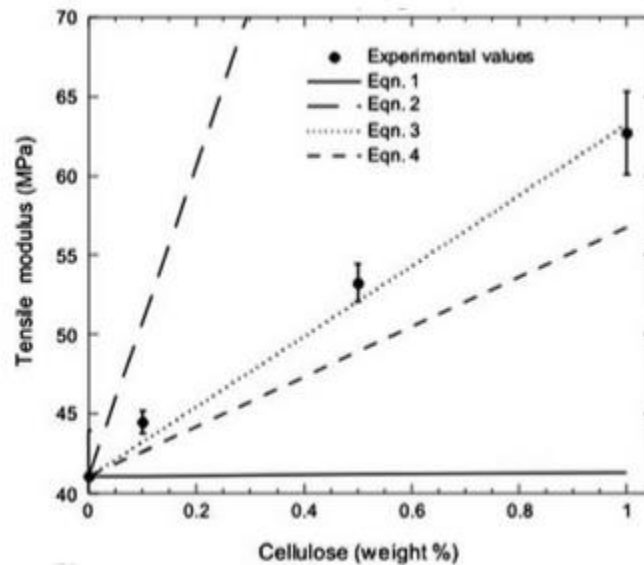


**Figure 2.** Tensile modulus as a function of the cellulose concentration.

To understand the unusual reinforcing effect observed at such low cellulose concentrations, a comparison between experimental results and different theoretical model calculations was performed. The moduli predicted by Eqns (1)–(4) were calculated for the present system and are included in Fig. 2. The experimentally measured value for 0 wt% cellulose was used as  $E_m$ . Regarding  $E_f$ , Favier et al.<sup>19</sup> indicate that the rigidity of the network of cellulose embedded crystallinities, which obviously differs from that of isolated whiskers, can be estimated by measuring the elastic properties of a film made only of cellulose whiskers. Using this approach they found a Young's modulus of 15 GPa measured experimentally in tension. This value, which is also an average value from literature values,<sup>19, 27–29</sup> was selected as  $E_f$ .

The calculated moduli from the Reuss and Voigt predictions are completely unsatisfactory, since the models are too simple for a composite with a three-dimensional arrangement of short fibers (nanocrystals). The Pan model predicts values that are closer but still lower than those of the real system. On the other hand, if the aspect ratio of the crystals ( $L/D$ ) is left to be a fitting parameter in



Eqn (4), a good agreement is found with  $L/D = 52$ , a value very close to others reported in the literature.<sup>19</sup>

### Creep behaviour

The creep behavior of the nanocellulose film composites was studied. In general, a curve of creep strain versus time can be considered as consisting of four stages: (i) initial rapid elongation, (ii) primary creep, (iii) secondary creep and (iv) tertiary creep.<sup>9, 30</sup> The initial rapid elongation is due to the elastic and plastic deformation of the polymer specimen, once a constant stress is applied; this stage is independent of time. The primary creep stage is a region of creep rate decreasing with time, which may be due to slippage and reorientation of polymer chains under persistent stress. After that, the creep rate reaches a steady-state value, secondary creep stage, which can occur over a long period of time. Finally, the material falls into the tertiary creep stage, where the creep rate increases rapidly, and finally creep fracture occurs.<sup>9</sup>

In order to select the conditions for creep testing inside the linear viscoelastic range, isochronous experiments were initially carried out.<sup>31</sup> From a set of creep curves obtained at different constant applied stresses, strain–stress plots were constructed at different selected times. The isochronous curves were found to be linear up to certain stress and strain levels. Figure 3 shows results for pure PU obtained from tests conducted at 20 °C for 60 min. From the analysis of the isochronous tests for the unreinforced PU (the sample showing the largest creep deformation) a stress of 500 kPa was selected for testing all the samples.

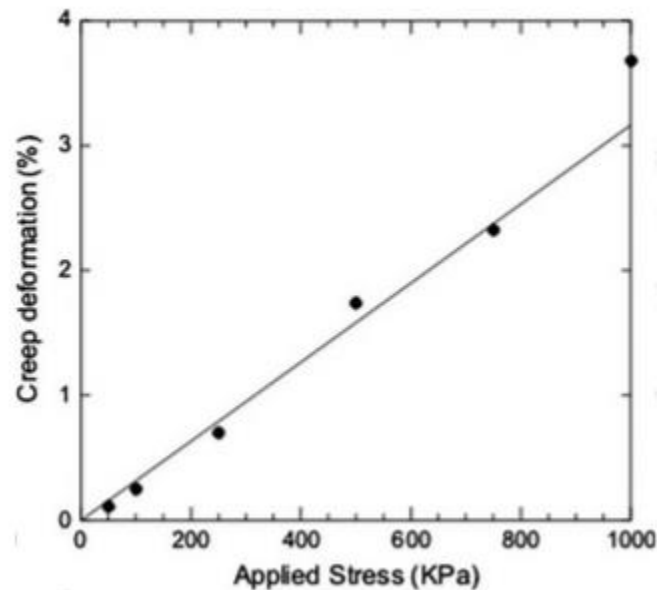
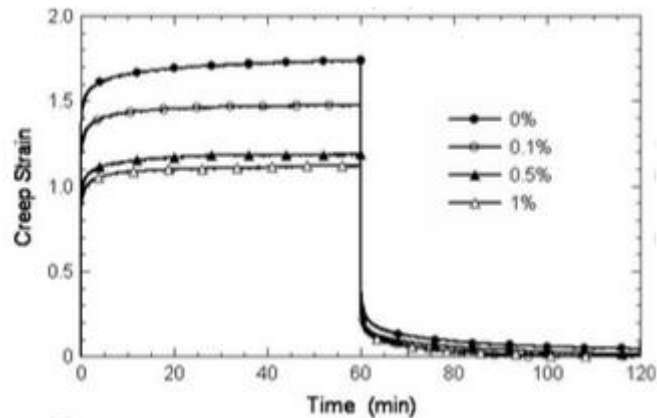


Figure 3. Isochronous (60 min) strain–stress plot for the unfilled PU.

The effect of the addition of nanocellulose on the tensile creep behavior of the PU at 20 °C is shown in Fig. 4. The creep strain decreases as cellulose concentration increases, despite the small amount of cellulose nanocrystals added. The effect of adding 0.1 and 0.5 wt% nanocellulose is quite important. In the last case, the creep strain after 60 min decreased from 1.74% for the neat matrix to 1.19% for the composite. However, increasing the cellulose concentration to 1 wt% produces only a marginal additional reduction, lowering the 60 min creep strain of the composite to 1.13%.



**Figure 4.** Creep curves for the unfilled PU and the nanocellulose-reinforced composites at 20 °C and a constant stress of 500 kPa (percentages expressed by weight).

Assuming efficient filler wetting and dispersion, cellulose addition is expected to stiffen the composite, since the reinforcement is stiffer than the matrix. Nanoparticles restrict the slippage, reorientation and general mobility of polymer chains. In this way, they influence the stress transfer, which ultimately results in the mentioned enhancement of the creep resistance.<sup>9</sup> The results support the physical picture of well-dispersed nanocellulose, which acts very efficiently in reducing the creep deformation of the composite films.

#### Thermomechanical cyclic tensile testing: shape memory behaviour

The shape memory behavior of the PU and nanocomposites was studied through thermomechanical experiments. Figure 5 presents the tensile stress–strain response coupled to the thermal cycling for the matrix and the composites. The behavior of the neat PU was equivalent, at least qualitatively, to that of the filler composites. The stress–strain response showed an elastic region followed by nonlinear deformation. During unloading, a small recovery occurred, so that the maximum deformation achieved could not be completely retained, as has been observed by other authors.<sup>4</sup> Additionally, upon heating, the original shape was not fully recovered, leaving a residual



deformation ( $\epsilon_p$ ). In all cases, the stress–strain behavior during the first cycle was distinct from the behavior observed in subsequent cycles, an usual behavior for this type of material.

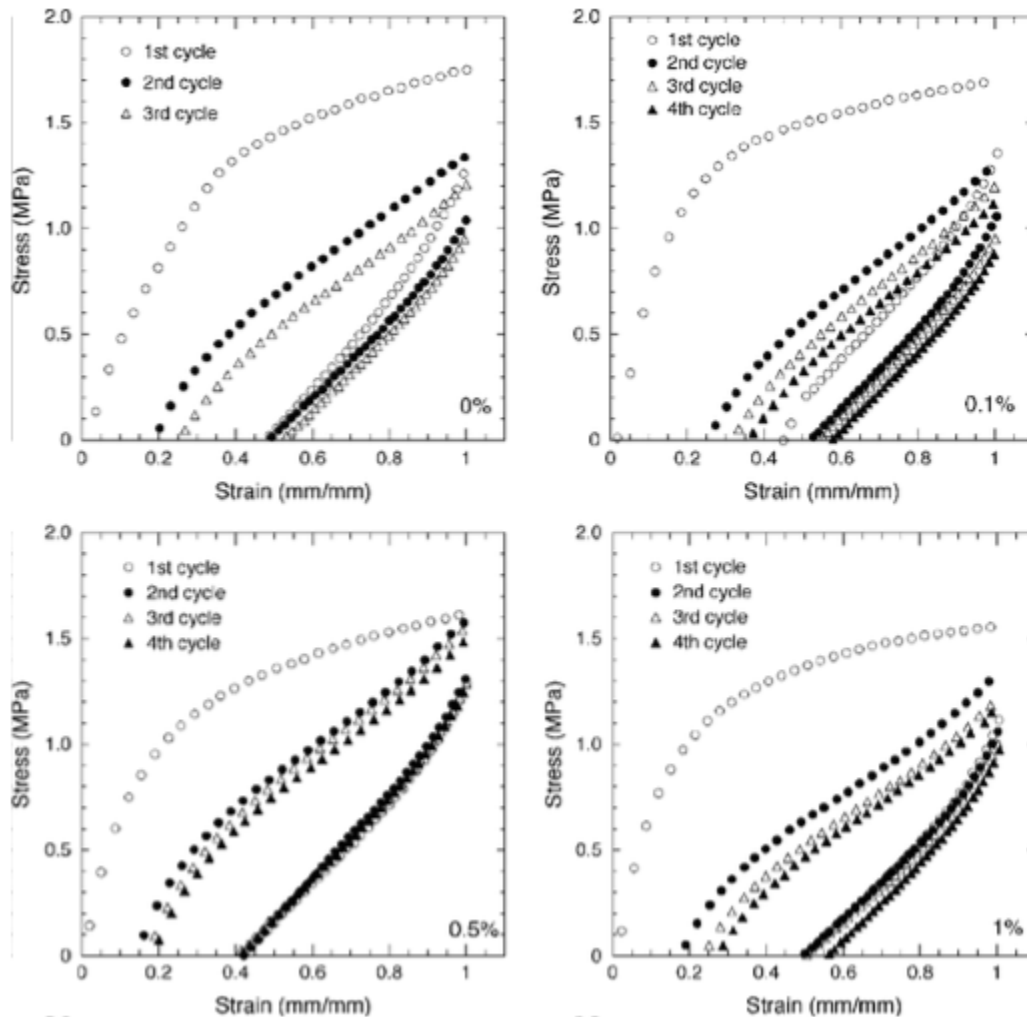


**Figure 5.** Thermal tensile cycles for unfilled PU and nanocellulose-reinforced PU.

The temperature selected for the shape memory testing was  $T_s = 60\text{ }^\circ\text{C}$ , an intermediate temperature between the melting temperature of the soft segments ( $T_{m,s} = 41\text{--}43\text{ }^\circ\text{C}$ ) and the melting temperature of the hard segments ( $T_{m,h} = 137\text{--}143\text{ }^\circ\text{C}$ ). In this range of temperatures, the material shows rubber elasticity due to the mobility of the amorphous phase of the soft segments and the restricted molecular motion imposed by the crystalline frozen phase. After being deformed at  $T_s$  and

subsequently cooled below  $T_{m,s}$  under constraint, the deformed shape was fixed to a large extent. Please cite this article as: M. L. Auad, V. S. Contos, S. Nutt, M.I. Aranguen, and N.E. Marcovich, “Characterization of Nano-Cellulose Reinforced Shape Memory Polyurethanes,” *Polymer International* 57 [4] (2008) 651-659. DOI: <http://dx.doi.org/doi:10.1002/pi.2394>



because of the frozen micro-Brownian movement of the chains. When they were reheated at  $T_s$ , the original shape was substantially recovered due to the elastic energy stored during the deformation process.<sup>5</sup>

Another interesting characteristic of this type of testing is the observed difference between the response in the first cycle as compared to subsequent cycles. This material response is common in thermoplastic elastomers and is attributed to the effect of the thermomechanical history on chain conformation and crystallite distribution.<sup>32</sup> The cyclic deformation response of a material depends on entanglement decoupling of molecular chains, orientation of molecular chains and hardening due to crystallization.<sup>2</sup> The response of the material is expected to be repeated after the second cycle.

The calculated shape memory properties (shape recovery and shape fixity) of all the samples are presented in Table 2. As observed in Fig. 5, the fixity increased (or remained largely unaffected) for the composites as well as for the unfilled PU. Although some variations of the fixity and recovery ratios were observed at the different cellulose concentrations, the differences between the calculated ratios for the neat PU and the 1 wt% sample did not differ markedly (Table 2). Additionally, the shape recovery ratio increases as the number of loading cycles increases. Large recovery values were obtained in and after the second cycle (Eqn (6)), reaching values in the range 93–98%.

*Table 2. Shape memory properties of cellulose-reinforced PU*

Cellulose fibers (wt%)	First cycle		Second cycle		Third cycle	
	$R_f$	$R_r(1)$	$R_f$	$R_r(2)$	$R_f$	$R_r(3)$
0	47.72	81.04	48.40	92.25	52.36	97.91
0.1	49.80	74.50	52.20	91.14	54.90	93.80
0.5	41.28	85.48	40.92	96.68	41.10	98.26
1.0	49.40	82.16	49.04	92.60	49.52	95.27



The observed increase of the recovery ratios when calculated with respect to the deformation of the previous cycles has been previously reported.<sup>2, 33</sup> Since the cyclic response tends to be more repeatable after the first deformation, the calculated ratios also become more repeatable.

Although the rigidity of the composites was markedly improved by the addition of nanocellulose (increased modulus, reduced creep), a characteristic that may have a positive effect on the long-term stability of the material, the deformability capacity of the composites did not change (tensile and cyclic tensile response). The improved rigidity did not have any substantial effect on the shape fixity or recovery of the material, either. The shape memory behavior continued to be controlled by the polymer properties under the testing conditions. The differences observed in the crystalline phase when nanocellulose is added may be obscured by the controlling kinetics of crystallization in the relatively faster cyclic tensile testing. Further studies to elucidate this matter are being conducted and will be the subject of a future publication.

## 4. CONCLUSIONS

SEM observations of SMP composites indicate that the size of the fibrils in composite films is comparable to the size of cellulose crystals. At concentrations as low as 1 wt%, the nanofibrils span the whole sample and a relatively uniform dispersion is observed through the entire film.

The phase separation of the crystalline regions corresponding to the soft segment chains was enhanced by the addition of small amounts of nanocellulose, and this was confirmed by DSC and WAXS experiments. DSC revealed that this effect is increased as cellulose concentration increased, with the 1 wt% sample showing the highest heat of melting of the soft segment crystals (increase of about 80% with respect to the neat PU sample). Additionally, as more cellulose was added to the nanocomposite, the spacing between soft segment crystalline planes became smaller (less disturbed



structure, better formed crystals). Thus, both techniques indicate that cellulose favors the formation of PU soft segment crystals.

Dynamic mechanical analysis results showed a slight increase in the position of the  $\tan \delta$  peak as the nanocellulose content increased. The height of the peak decreased in a proportion larger than expected from a simple dilution effect (from 0.29 to 0.21 with the addition of 1 wt% cellulose), which was the result of the large and strong interfacial interactions developed between nanocellulose fibers and PU matrix.

The general trend indicates that tensile modulus increased as cellulose fiber content increased, while the creep deformation decreased with increasing nanocellulose loadings. Addition of just 1 wt% of nanocellulose resulted in a tensile modulus increase of about 53% and creep reduction of about 36%. Both effects were the result of the incorporation of a rigid, well-dispersed nanoreinforcement to the elastomeric PU matrix. In both cases, the changes introduced are very large considering the small amount of cellulose nanocrystals added in the nanocomposites formulation.

The cellulose nanocrystal composites displayed essentially the same shape memory properties as those corresponding to neat PU. The recovery of shape is quite large and repeatable after the second cycle for all the materials. These results indicate that PU polymer controls this behavior under the conditions of temperature and deformation imposed in the tensile cycling, and that the addition of the nanocrystals does not inhibit the shape memory response.

**Acknowledgements:** NEM thanks the Science and Technology National Promotion Agency (ANPCyT) for grant PICT no. 14604. The authors thank the financial support of the National Research Council of Argentina (CONICET) and National University of Mar del Plata (UNMdP). SRN gratefully acknowledges support from the Merwyn C Gill Foundation. Thanks are also due to Huntsman Polyurethanes for supplying the shape memory polymer utilized in this work.

Please cite this article as: M. L. Auad, V. S. Contos, S. Nutt, M.I. Aranguen, and N.E. Marcovich, “**Characterization of Nano-Cellulose Reinforced Shape Memory Polyurethanes,**” *Polymer International* 57 [4] (2008) 651-659. DOI: <http://dx.doi.org/doi:10.1002/pi.2394>



## References:

- 1 Wei ZG, Sandstrom R and Miyazaki S, *J Mater Sci* 33:3743 (1998).
- 2 Tobushi H, Hara H, Yamada E and Hayashi S, *Smart Mater Struct* 5:483 (1996).
- 3 Li F, Zhang X, Hou J, Xu M, Luo X, Ma D, et al, *J Appl Polym Sci* 64:1511 (1997).
- 4 Gall K, Dunn ML, Liu Y, Finch D, Lake M and Munshi NA, *Acta Mater* 50:5115 (2002).
- 5 Jeong HM, Lee SY and Kim BK, *J Mater Sci* 35:1579 (2000).
- 6 Kim BK, Sang YL and Xu M, *Polymer* 37:5781 (1996).
- 7 Liu Y, Gall K, Dunn ML and McCluskey P, *Smart Mater Struct* 12:947 (2003).
- 8 Vlasveld DPN, Bersee HEN and Picken SJ, *Polymer* 46:12539 (2005).
- 9 Zhang Z, Yang J-Y and Fiedrich K, *Polymer* 45:3481 (2004).
- 10 Nunes RCR, Fonseca JLC and Pereira MR, *Polym Testing* 19:93 (2000).
- 11 Eichhorn SJ and Young RJ, *Cellulose* 8:197 (2001).
- 12 Zadorecki P and Michell A, *Polym Compos* 10:69 (1989).
- 13 Boldizar A, Klason C, Kubat J, Naslund P and Saha P, *Int J Polym Mater* 11:229 (1987).
- 14 Woodhams RT, Thomas G and Rogers DK, *Polym Eng Sci* 24:1166 (1984).
- 15 Gouss e C, Chanzy H, Cerrada ML and Fleury E, *Polymer* 45:1569 (2004).
- 16 Marcovich NE, Bellesi NE, Auad ML, Nutt SR and Aranguen MI, *J Mater Res* 21:870 (2006).
- 17 Marcovich NE, Aranguen MI and Reboledo MM, *Polymer* 42:815 (2001).
- 18 Dufresne A and Cavaill eJ-Y, *J Polym Sci B: Polym Phys* 36:2211 (1998).
- 19 Favier V, Canova GR, Shrivastava SC and Cavaill eJY, *Polym Eng Sci* 37:1732 (1997).
- 20 Pan, N. *Sci. Eng. Compos. Mater.* 5:63 (1996).
- 21 Ebeling T, Paillet M, Borsali R, Diat O, Dufresne A, Cavaill eJ-Y, et al, *Langmuir* 15:6123 (1999).
- 22 Podsiadlo P, Choi S-Y, Shim B, Lee J, Cuddihy M and Kotov NA, *Biomacromolecules* 6:2914 (2005).
- 23 Nunes RCR, Pereira RA, Fonseca JLC and Pereira MR, *Polym Testing* 20:707 (2001).
- 24 Mathew AP and Dufresne A, *Biomacromolecules* 3:609 (2002).
- 25 Ryabov SV, Kercha YY, Kotel'nikova NE, Gaiduk RL, Shtom-pel VI, Kosenko LA, et al, *Polym Sci Ser A* 43:1256 (2001).
- 26 Song YS and Youn LR, *Carbon* 43:1378 (2005).
- 27 Azizi Samir MAS, Alloin F, Sanchez J-Y, El Kissi N and Dufresne A, *Macromolecules* 37:1386 (2004).
- 28 Yamanaka S, Watanabe K, Kitamura N, Iguchi M, Mitsuhashi S, Nishi Y, et al, *J Mater Sci* 24:3141 (1989).
- 29 Favier V, Chanzy H and Cavaill eJY, *Macromolecules* 28:6365 (1995).
- 30 ASTM D 2990-01.
- 31 Marais C and Villoutreix G, *J Appl Polym Sci* 69:1983 (1998).
- 32 Boyce MC, Socrate S, Kear K, Yeh O and Shaw K, *J Mech Phys Solids* 49:1323 (2001).
- 33 Lin JR and Chen LW, *J Appl Polym Sci* 69:1563 (1998).